

## Making Metals Transparent for White Light by Spoof Surface Plasmons

Xian-Rong Huang,<sup>1,\*</sup> Ru-Wen Peng,<sup>2,†</sup> and Ren-Hao Fan<sup>2</sup>

<sup>1</sup>*Advanced Photon Source, Argonne National Laboratory, Argonne, Illinois 60439, USA*

<sup>2</sup>*National Laboratory of Solid State Microstructures and Department of Physics, Nanjing University, Nanjing 210093, China*  
(Received 10 May 2010; revised manuscript received 4 November 2010; published 7 December 2010)

From first-principles computations we reveal that metallic gratings consisting of narrow slits may become transparent for extremely broad bandwidths under oblique incidence. This phenomenon can be explained by a concrete picture in which the incident wave drives free electrons on the conducting surfaces and part of the slit walls to form spoof surface plasmons (SSPs). The SSPs then propagate on the slit walls but are abruptly discontinued by the bottom edges to form oscillating charges that emit the transmitted wave. This picture explicitly demonstrates the conversion between light and SSPs and indicates clear guidelines for enhancing SSP excitation and propagation. Making structured metals transparent may lead to a variety of applications.

DOI: 10.1103/PhysRevLett.105.243901

PACS numbers: 42.25.Bs, 42.79.Dj, 78.67.-n, 84.40.Az

Interactions between light and conducting nanostructures can give rise to various unexpected and fascinating phenomena through surface plasmons (SPs), which have numerous (potential) applications. In fact, the seminal work of extraordinary optical transmission by Ebbesen *et al.* [1] opened up a new and exciting avenue in *plasmonics*, which recently has been further extended to many other fields. In the large literature (e.g., see [2]), a variety of conducting structures have been studied both theoretically and experimentally, from which it is generally admitted that SPs play the essential role through the process that the incident light is first converted to SPs, which then propagate along the conducting surfaces, slit or hole walls, nanowires, channels, etc., before being converted back into light [3]. Although this mechanism is widely accepted, a clear picture about exactly how light is converted to SPs [or spoof SPs (SSPs) [4] for highly conducting structures] and vice versa is still under investigation.

Nevertheless, the plasmonic field is advancing rapidly, but most of the research has been based on the “generate and test” search procedure because of the unclear mechanism of conversion between light and SPs. In our recent work [5,6], we have illustrated from a different viewpoint a basic picture about interaction between light and conducting microstructures. When light is incident on a highly conducting surface, it drives free surface electrons to move, but the moving electrons can be impeded by the rough parts (e.g., grooves, holes, and particles) of the surface to form charge patterns. The agitated electrons may also propagate away on the conducting surface as subwavelength surface charge density waves. When the propagation is discontinued, the charge waves are converted back to oscillating charge patterns. All the charge patterns are light sources emitting new wavelets. It is the new wavelets and/or their interference that give rise to anomalous transmission, reflection, or scattering.

Here we demonstrate that this mechanism can make one-dimensional (1D) highly conducting gratings transparent for nearly white spectra. Our purpose is threefold. First, we show that plasmonics is really a fantastic field that is far from completely understood. The optical properties of even the simplest structured conductors have not been fully explored. Second, making metals transparent may lead to a variety of applications, including white-beam polarizers, antireflection materials, cloaking, transparent windows with embedded electrodes or antennas [7], etc. Third, the conducting grating is one of the simplest plasmonic materials, involving only a few electrodynamic mechanisms, from which the SP or SSP mechanisms can be easily singled out.

The simple 1D periodic slit arrays we studied is illustrated in the inset in Fig. 1(a) with  $d$ ,  $W$ , and  $\tau$  denoting the grating period, the slit width, and the grating thickness, respectively. The electrostatics of this structure can be accurately computed by the rigorous coupled-wave analysis (RCWA) [6,8,9]. Figure 1(a) shows the calculated transmission curves of a gold grating with the incident angle  $\theta$  being 0 (normal incidence) and 60°, respectively, at  $\tau = 10 \mu\text{m}$  [10]. The transmission peaks are well known to be Fabry-Perot (FP) resonance peaks [2,5,6,11,12]. In particular, the normal-incidence transmissivity pattern has been precisely verified by experiments at microwave frequencies (see [13,14]).

In Fig. 1(a), one can see that the overall transmissivity  $T_0$  increases with increasing incident angle  $\theta$ . This is counterintuitive, because, for a flat and homogenous surface, it is the reflectivity ( $R_0$ ) that generally increases with increasing  $\theta$  (while  $T_0$  decreases). When  $\theta$  is further increased to be around 84°, as shown in Fig. 1(b), it becomes more surprising that the FP peaks disappear and that the transmission curve becomes nearly flat in the long wavelength range  $\lambda > d(1 + \sin\theta) \approx 2d$ ; i.e., the grating becomes transparent for a white beam. Meanwhile, the

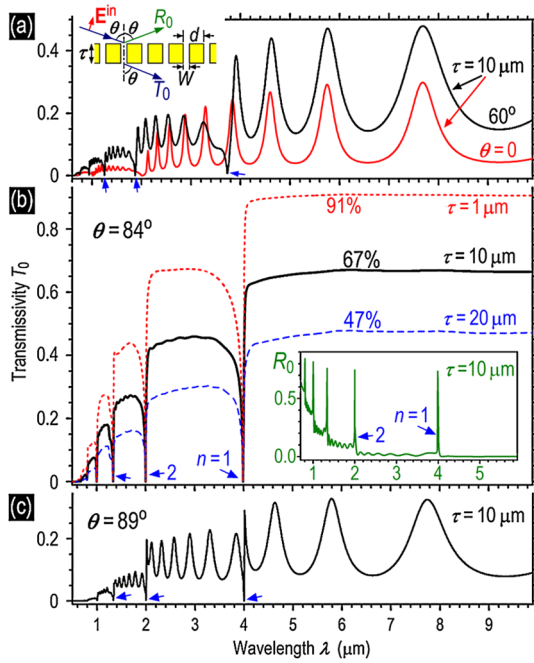


FIG. 1 (color online). Transmission spectra of a gold grating with  $d = 2 \mu\text{m}$  and  $W = 0.2 \mu\text{m}$  ( $W/d = 10\%$ ). TM polarization. (a) Transmission for normal and  $60^\circ$  incidence. (b) Maximized and flat transmission at  $\theta = 84^\circ$ . The inset shows the reflectivity for  $\tau = 10 \mu\text{m}$ . (c) Transmission for extremely grazing geometry.

inset in Fig. 1(b) shows that the reflectivity  $R_0$  is zero in this range. Note that  $\theta \sim 84^\circ$  corresponds to the grazing-incidence geometry, under which most flat surfaces are nearly totally reflective. But here light is completely transmitted or absorbed rather than being reflected. Our calculations show that the nearly flat transmission curves in Fig. 1(b) extend up to millimeter wavelengths except that overall  $T_0$  increases slowly with increasing  $\lambda$  [14].

As described in Ref. [6], the FP resonance peaks strongly depend on the grating thickness  $\tau$  (but nearly independent of  $\theta$ ) in the  $\lambda > d(1 + \sin\theta)$  range. However, when  $\theta \sim 84^\circ$ , the flat shape of the transmissivity becomes independent of  $\tau$ , as shown by the three  $T_0$  curves calculated with  $\tau = 1, 10,$  and  $20 \mu\text{m}$ , respectively, in Fig. 1(b). This means that the FP effect is absent at  $\theta \sim 84^\circ$ . In Fig. 1(b), the transmissivity of  $\sim 47\%$  at  $\tau = 20 \mu\text{m}$  is remarkable. Our calculations show that  $T_0$  remains above 10% until  $\tau > 65 \mu\text{m}$ . (For larger  $W/d$  ratios, the transmission thickness can be much larger.) With  $R_0$  always being zero,  $1 - T_0$  represents the Ohmic loss as the light scattering along directions other than the transmitted  $T_0$  direction is always zero for  $\lambda > d(1 + \sin\theta)$  [5,6].

In Fig. 1(c), when  $\theta$  is further increased towards  $90^\circ$ ,  $T_0$  drops again with the FP peaks reappearing. Hence,  $\theta \sim 84^\circ$  is the incident angle with maximum and “flat” transmission for the current lattice parameters. The arrowed transmissivity minima in Fig. 1 correspond to Wood’s anomalies occurring at  $d(1 + \sin\theta) = n\lambda$  ( $n = 1, 2, 3, \dots$ ), where the reflectivity is maximized [see the

inset in Fig. 1(b)]. The lower transmission in the  $\lambda \leq d(1 + \sin\theta)$  range (in which the grating is no longer a subwavelength lattice) is due to nonevanescent wave diffraction [6].

Note that the flat and strong transmission effect tends to be weak or disappear in the short wavelength range ( $\lambda < 1 \mu\text{m}$ ) even if the grating is still a subwavelength lattice [ $d < \lambda/(1 + \sin\theta)$ ], as can be verified by RCWA calculations. According to Refs. [4,15], the surface waves near a structured metal surface consist of two main components: One is the SP component that is dominant for short wavelengths, while the other is the geometrical SSP component that becomes outstanding in the long wavelength range where the metal is highly conductive. Therefore, for  $\lambda > d(1 + \sin\theta)$  in Fig. 1, light is transmitted through the 1D conducting gratings dominantly by SSPs, which are still subwavelength surface charge density waves but with detailed charge distributions.

Figure 2(a) shows the calculated charge densities on the top and bottom surfaces of the grating under the flat transmission condition of Fig. 1. Note that the charge densities oscillate with a time factor  $e^{i\omega t}$  ( $\omega$  the frequency of the incident wave). Here A, B, C, and D denote the four corners of a slit (see Fig. 3). One can see that inhomogeneous charge patterns appear on the surfaces. Particularly, the charges highly accumulate near the corners A and D.

Figure 2(b) shows the charge densities on the two walls of a slit, which again reveals the high charge densities near A and D. Between the two corners A and C (or B and D), the charge densities are nearly homogeneous. In terms of the wave phases in the inset, the charge waves on the two opposite walls are simple sinusoidal waves that can be written as  $\rho_w(z) \exp[i(\omega t - k_z z)]$  and  $-\rho_w(z) \exp[i(\omega t - k_z z)]$ , respectively (equal wave amplitudes but with a phase difference  $\pi$ ), where  $k_z = 0.281 \pi/\mu\text{m}$  and  $\rho_w(z)$  is nearly constant except that its magnitude slightly decays along  $+z$  due to Ohmic absorption. Accordingly, the electric field in the slit has the wave form  $\mathbf{E}_a(z) \exp[i(\omega t - k_z z)]$  (constant along  $x$ , waveguide mode) propagating toward  $+z$  [rather than the incidence direction; see Fig. 3(b)] with  $|\mathbf{E}_a(z)| \propto \rho_w(z)$ . Interestingly, the spatial period of the charge wave is  $\lambda_z = 2\pi/k_z = 7.1 \mu\text{m}$  [16], which is smaller than the incident wavelength  $\lambda = 8 \mu\text{m}$ . Therefore, the charge waves on the walls indeed have the subwavelength characteristics of SPs. Note that the wave  $\mathbf{E}_a(z) \exp[i(\omega t - k_z z)]$  propagates with a phase speed of  $c\lambda_z/\lambda = 0.89c$  in the vacuum space of the slit ( $c$  the normal speed of light in vacuum). The charge patterns on the top and bottom surfaces are not sinusoidal, with the period (always) equal to the lattice constant  $d = 2 \mu\text{m}$ , also less than  $\lambda$ .

Figure 3(b) schematically shows the charge distributions of Fig. 2. First let us briefly recall the normal-incidence case in Fig. 3(a). In this geometry, the incident electric field  $\mathbf{E}^{\text{in}}$  drives free electrons on the top surface AB to move, but the movement is stopped at one corner, resulting in accumulation of electrons there. Meanwhile, extra positive charges appear at the other corner since some of the

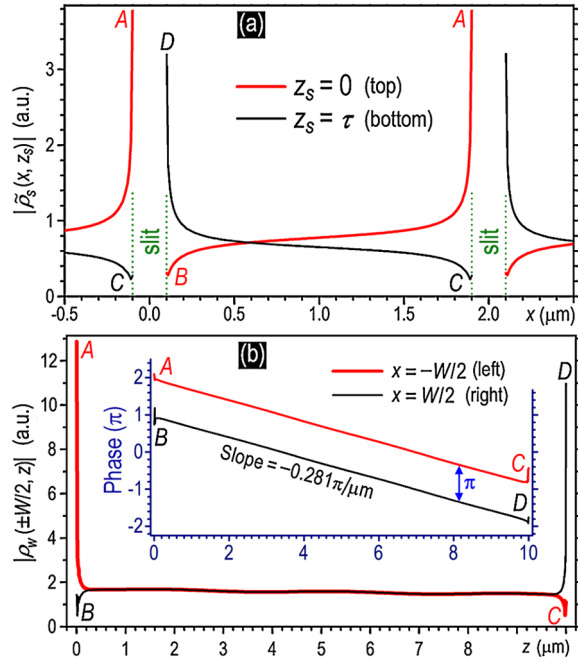


FIG. 2 (color online). Charge densities on the two grating surfaces (a) and on the two slit walls (b) for  $W = 0.2$ ,  $d = 2$ ,  $\tau = 10$ ,  $\lambda = 8 \mu\text{m}$ , and  $\theta = 84^\circ$  (flat transmission conditions).

electrons have moved away. Consequently, a dipole  $\mathbf{P}_a$  is formed, which oscillates with  $\mathbf{E}^{\text{in}}$  and emits a wavelet  $\mathbf{E}_a$  in the slit.  $\mathbf{E}_a$  then drives free electrons on the slit walls to form SSPs that propagate along  $+z$ . When the SSPs reach the bottom, the charge movement is stopped at corners  $C$  and  $D$  to form another dipole  $\mathbf{P}_b$ . Meanwhile, the charge waves are partly bounced back from these two corners, and  $\mathbf{P}_a$  and  $\mathbf{P}_b$  can thus form FP resonance [16]. The wavelets ( $T_0$ ) emitted from  $\mathbf{P}_b$  along  $+z$  then form the transmitted beam (see [5,6] for details).

Note that in Fig. 3(a) the incident beam only exerts a tangential driving force  $eE^{\text{in}}$  on the electrons on the top surface [ $e(<0)$  being the charge per electron]. The reason why most of the moving electrons are stopped at the corner instead of moving continuously onto the slit wall is due to the lack of a vertical driving force for the electrons to make an abrupt  $90^\circ$  turn around the corner. The activation of SSPs on the slit walls is dominantly driven by the wavelet  $\mathbf{E}_a$ , which is a secondary process that is very inefficient (with lower transmission) because the driving force exerted by  $\mathbf{E}_a$  is perpendicular to the walls.

By contrast, in the oblique-incidence geometry of Fig. 3(b), the incident beam directly illuminates part of the slit wall ( $BP$ ), which provides a vertical driving force (per electron)  $eE^{\text{in}} \sin\theta$  on the electrons on the wall. On the top surface, the driving force becomes  $eE^{\text{in}} \cos\theta$  and still drives the electrons to move, but now the electrons can move continuously around corner  $B$  due to the vertical driving force  $eE^{\text{in}} \sin\theta$  exerted on wall  $BP$ . This explains the absence of charge accumulation at corner  $B$  in Fig. 2. However, charge discontinuity and accumulation still occur at corner  $A$  since the incident wave provides no

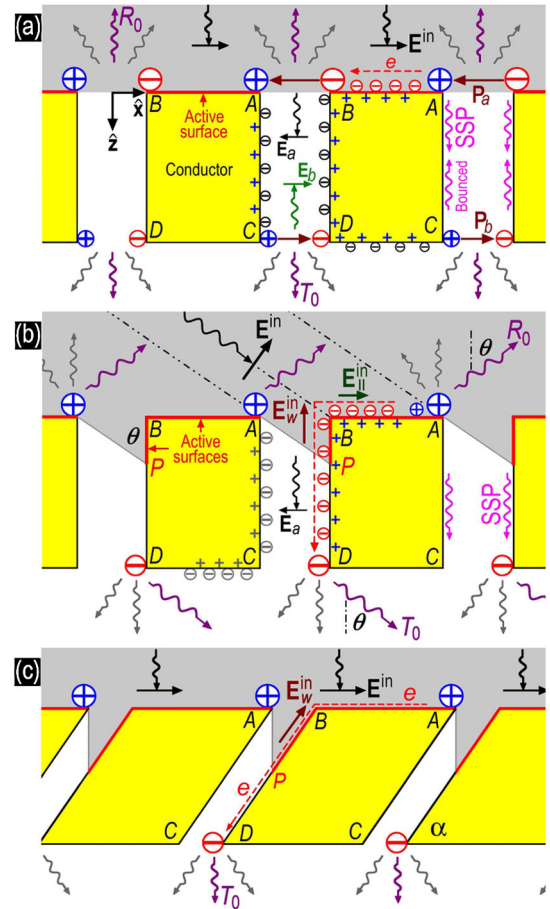


FIG. 3 (color online). Light transmission through conducting gratings. (a) Normal incidence. (b) Oblique incidence under the flat transmission condition.  $\mathbf{E}_w^{\text{in}}$  and  $\mathbf{E}_s^{\text{in}}$  are the projections of  $\mathbf{E}^{\text{in}}$  onto the surface and the slit wall, respectively. (c) Normal incidence for the oblique grating, where the transmitted beam ( $T_0$ ) is still vertical.

driving force on wall  $AC$ . The charge waves formed on the active surfaces  $AB$  and  $BP$  then continuously propagate on the unilluminated wall  $PD$  as an SSP, but the moving charges are stopped and accumulated at corner  $D$  in the absence of direct driving forces on  $CD$ . Note that the charge wave on wall  $AC$  (also appearing as an SSP with an opposite phase) is passively activated by the electric field  $\mathbf{E}_a$  to satisfy the waveguide mode in the slit.

On the top surface, the charges near corner  $A$  oscillate with the incident wave and consequently emit new wavelets. As described in Ref. [6], only along the specular reflection direction ( $R_0$ ) are the wavelets emitted from adjacent slits *in phase*, which form the propagating reflected wave. Under the flat transmission condition of Fig. 1(b), these wavelets completely offset the wavelets specularly reflected from the surfaces ( $AB$ ), thus resulting in zero reflectivity [see the inset in Fig. 2(b)]. Wavelets along other directions are always out of phase and form evanescent waves. Similarly, the wavelets emitted from corners  $D$  form the transmitted wave along the transmission direction ( $T_0$ ). (Note that no specular reflection exists on the bottom surface.) The charge patterns

on the bottom surface  $CD$  are passively activated by the near electromagnetic fields from  $D$  to satisfy the boundary conditions.

For normal incidence in Fig. 3(a), the SSPs on the slit walls are always bounced back from  $C$  and  $D$ , and the forward and backward SSPs then form standing charge waves on the walls [6], which can give rise to the FP resonance transmission peaks. Under the flat transmission condition for oblique incidence, however, Fig. 2(b) shows that the backward SSPs are absent. The reason is that the tendency for the SSP to be bounced back in Fig. 3(b) is suppressed by the force  $eE^{\text{in}} \sin\theta$  exerted on the electrons on wall  $BP$ . Similarly, the force  $eE^{\text{in}} \cos\theta$  on  $AB$  suppresses the tendency for the charge waves to be bounced back from  $A$ . Note that the magnitudes of both forces depend on the incident angle  $\theta$ . Figures 1 and 2 indicate that there exists a balanced angle  $\theta_f (= 84^\circ)$ , near which the two forces completely suppress the bouncing-back tendency of the moving electrons at both  $A$  and  $D$ . Under this condition, the transmission is maximized and flat. Out of this balanced condition, there always exists a bounced SSP on the slit wall (due to under- or oversuppression), which leads to the oscillating transmission curves.

Nevertheless, since in the oblique-incidence geometry the incident wave always provides a direct driving force on the slit walls to enhance the excitation of SSPs, the transmission efficiency is almost always greater than the normal-incidence case, as shown in Figs. 1(a) and 1(b) for  $\tau = 10 \mu\text{m}$ . The exception is that under extremely grazing geometry where the illuminated depth of the slit walls [ $BP$  in Fig. 3(b)] becomes very small, this enhanced transmission effect tends to disappear, as shown in Fig. 1(c).

Although  $\theta_f$  can be numerically calculated by RCWA, we may obtain an empirical equation for predicting it. Note that in Fig. 3 the *total force* exerted by the incident wave on all the free electrons on the wall  $BP$  may be written as  $F_1^{\text{tot}} = (eE^{\text{in}} \sin\theta)l_1I_1$ , where  $l_1 = W \tan^{-1}\theta$  is the illuminated depth  $BP$  and  $I_1 \propto \sin\theta$  is the photon density incident on the wall  $BP$ . Accordingly, the total force exerted on the upper surface  $AB$  is  $F_2^{\text{tot}} = (eE^{\text{in}} \cos\theta)l_2I_2$ , where  $l_2 = d - W$  and  $I_2 \propto \cos\theta$ . For highly conducting metals at long wavelengths, since the response of the electrons is so fast that all retardation effects are usually negligible, we may assume that the two forces should be equal at  $\theta_f$  so that the charges can smoothly move across the corner  $B$  without accumulation. Then  $F_1^{\text{tot}} = F_2^{\text{tot}}$  leads to an approximate guideline

$$\tan\theta_f \simeq (d - W)/W. \quad (1)$$

As an example, for  $d = 2$  and  $W = 0.2 \mu\text{m}$ , Eq. (1) predicts  $\theta_f = 83.7^\circ$ , which is very close to the RCWA result  $\theta_f = 84^\circ$  in Fig. 1. Although extremely simple, Eq. (1) works quite well for highly conducting gratings (see [14] for more details).

Thus, we have demonstrated a concrete SSP picture about light transmission through 1D conducting gratings, from which one can see clearly the mechanism underlying the

conversion between light and SSPs and how the conversion efficiency and the SSP propagation can be enhanced. We believe that this picture can provide straightforward guidelines for designing useful plasmonic devices. For example, we have mentioned above that transparent structured metals have a variety of applications, but the oblique-incidence geometry may not be desirable in many cases. Based on the above picture, however, we predict that the design of oblique gratings, as shown in Fig. 3(c), may achieve flat and maximum transmission under normal incidence. The mechanism here is obvious as the incident wave again directly illuminates the slit wall ( $BP$ ) and provides a direct tangential driving force to enhance the excitation of SSPs on the walls. Details will be presented elsewhere.

We are grateful to Professor P. Lalanne for very helpful suggestions and discussions. This work was supported by the U.S. Department of Energy, Office of Science, Office of Basic Energy Sciences, under Contract No. DE-AC02-06CH11357, and by grants from the NSFC (Grants No. 10625417, No. 11034005, No. 61077023, and No. 11021403), the MOST of China (Grant No. 2010CB630705), and partly by Jiangsu Province (BK2008012).

\*xiahuang@aps.anl.gov

†rwpeng@nju.edu.cn

- [1] T. W. Ebbesen *et al.*, *Nature (London)* **391**, 667 (1998).
- [2] F. J. Garcia-Vidal *et al.*, *Rev. Mod. Phys.* **82**, 729 (2010).
- [3] W. L. Barnes, A. Dereux, and T. W. Ebbesen, *Nature (London)* **424**, 824 (2003).
- [4] J. B. Pendry, L. Martín-Moreno, and F. G. Garcia-Vidal, *Science* **305**, 847 (2004).
- [5] X. R. Huang *et al.*, *Phys. Rev. A* **76**, 035802 (2007).
- [6] X.-R. Huang and R.-W. Peng, *J. Opt. Soc. Am. A* **27**, 718 (2010).
- [7] Z. J. Zhang *et al.*, *Appl. Phys. Lett.* **93**, 171110 (2008).
- [8] P. Lalanne and G. M. Morris, *J. Opt. Soc. Am. A* **13**, 779 (1996).
- [9] B. Guizal, H. Yala, and D. Felbacq, *Opt. Lett.* **34**, 2790 (2009).
- [10] *Handbook of Optical Constants and Solids*, edited by E. D. Palik (Academic, Orlando, 1985).
- [11] J. R. Suckling *et al.*, *Phys. Rev. Lett.* **92**, 147401 (2004).
- [12] J. A. Porto, F. J. García-Vidal, and J. B. Pendry, *Phys. Rev. Lett.* **83**, 2845 (1999); Q. Cao and P. Lalanne, *ibid.* **88**, 057403 (2002).
- [13] H. E. Went *et al.*, *Appl. Phys. Lett.* **77**, 2789 (2000).
- [14] See supplementary material at <http://link.aps.org/supplemental/10.1103/PhysRevLett.105.243901> for discussions of RCWA, wavelength extension, and  $\theta_f$ .
- [15] H. Liu and P. Lalanne, *Nature (London)* **452**, 728 (2008).
- [16] Calculations show that  $\lambda_z$  is an intrinsic property of the slit, only depending on  $\lambda$ ,  $W$ , and the permittivity while independent of other parameters (including  $\theta$ ). This is also true for isolated slits.  $\lambda_z < \lambda$  directly leads to the redshift of the FP resonance peaks (i.e., occurring at  $N\lambda_z = 2\tau$  rather than  $N\lambda = 2\tau$ ) [6,11].